CMLS, Cell. Mol. Life Sci. 60 (2003) 176–184
1420-682X/03/010176-09

CMLS Cellular and Molecular Life Sciences

Research Article

Solution structure and activity of mouse lysozyme M

T. Obita, T. Ueda* and T. Imoto

Graduate School of Pharmaceutical Sciences, Kyushu University, 3-1-1 Maidashi, Higashi-ku, Fukuoka 812-8582 (Japan), Fax: +81 92 642 6667, e-mail: ueda@phar.kyushu-u.ac.jp

Received 18 September 2002; received after revision 25 October 2002; accepted 13 November 2002

Abstract. The three-dimensional structure of mouse lysozyme M, glycoside hydrolase, with 130 amino acids has been determined by heteronuclear NMR spectroscopy. We found that mouse lysozyme M had four α-helices, two 3_{10} helices, and a double- and a triple-stranded anti-parallel β-sheet, and its structure was very similar to that of hen lysozyme in solution and in the crystalline state. The pH activity profile of *p*-nitrophenyl penta N-acetyl-β-D-chitopentaoside hydrolysis by mouse lysozyme M was similar to that of hen lysozyme, but the hydrolytic activity of mouse lysozyme M was lower. From analyses of binding affinities of lysozymes to a substrate analogue and internal motions of lysozymes, we suggest that the lower activity of mouse lysozyme M was due to the larger dissociation constant of its enzyme-substrate complex and the restricted internal backbone motions in the molecule.

Key words. Activity; internal motion; mouse lysozyme M; NMR; solution structure.

Lysozyme is an enzyme that catalyzes the hydrolysis of a co-polymer of N-acetylmuramic acid and N-acetylglucosamine and a polymer of N-acetylglucosamine [1]. Lysozyme plays an early role in host defenses and can be found in most tissues in animals. In the house mouse, the closely related mouse lysozymes M and P tend to be expressed in different tissues; mouse lysozyme M is strongly expressed in both macrophages and macrophage-rich tissues, while mouse lysozyme P is mainly expressed in the small intestine [2]. Recently, our group showed that mutant mouse lysozyme M evoked a strong autoantibody response [3], and we obtained autoantibody for native mouse lysozyme M. However, the three-dimensional structure of mouse lysozyme M has not yet been investigated via X-ray crystallography or nuclear magnetic resonance (NMR), meaning that we cannot yet understand the biological significance of the autoantibody on the basis of protein structure.

* Corresponding author.

The biological activity of mouse lysozyme M has also not been investigated in detail. A comparative biological study has given us much information about protein functions. Therefore, to determine the enzymatic reaction mechanism of mouse lysozyme M, we compared the biological activity and backbone dynamics of mouse lysozyme M with those of hen lysozyme, whose enzymatic reaction mechanism has been investigated in detail, by means of a physico-chemical method and NMR. Here we report the solution structure of mouse lysozyme M at pH 3.8 and 35 °C based on the heteronuclear NMR method, and we describe the activity, substrate binding, and backbone dynamics of mouse lysozyme M.

Materials and methods

Materials

Hen egg white lysozyme was obtained from QP Co. (Tokyo, Japan). Trimer of N-acetyl glucosamine, $(GlcNAc)_3$ and p-nitrophenyl penta N-acetyl-β-D-chitopen-

taoside [PNP-$(GlcNAc)_5$] were purchased from Seikagaku Kogyo (Tokyo, Japan). YMC-pack A-014 (6 × 300 mm) column was purchased from Yamamura Kagaku Kogyo (Kyoto, Japan). All other chemicals were of analytical grade for biochemical use.

Sample preparation

Mouse lysozyme M was obtained from the *Pichia pastoris* expression system, as described in our previous paper [4]. Briefly, the ^{15}N-labeled protein was expressed in FM22-glycerol minimal medium (100 ml of 10% glycerol, 1 ml of PTM1, 6 ml of 250 × biotin, and 6 ml of 10 M KOH were added to 1000 ml of FM22) containing $(^{15}NH_4)_2SO_4$ as the sole nitrogen source. The protein was purified by cation exchange (CM-Toyopearl 650M) chromatography. The yield of purified protein was about 10 mg per liter of culture.

NMR measurements

NMR measurements were performed on a Varian Inova 600 NMR spectrometer. $^1H-^{15}N$ HSQC spectra of mouse lysozyme M with or without a large excess of $(GlcNAc)_3$, a substrate analogue of lysozyme, were measured at 35 °C in 90% H_2O/10% D_2O (v/v) at a protein concentration of 1.0 mM, and the pH was adjusted to 3.8 as described in our previous report [5]. The distance restraints were obtained from ^{15}N-edited NOESY (80 and 120 ms mixing time) and ^1H NOESY (120 ms mixing time). The acquisition time for ^{15}N-edited NOESY was about 4 days. For the H-D exchange experiment, we measured $^1H-^{15}N$ HSQC spectra at 3 and 24 h after dissolving lyophilized mouse lysozyme M in D_2O. To calculate the structure, 1321 distance restraints were supplemented with angle restraints based on HNHA data and hydrogen bond restraints based on solvent exchange experiments. The three-dimensional structure of mouse lysozyme M was computed using DYANA [6]. Co-ordinates of the 20 final structures have been deposited in the Protein Data Bank (accession code 1IVM).

We obtained the dissociation profile of the acidic residues in the lysozyme from pH titration of acidic residues in mouse lysozyme M using the following equation [7]:

$$\delta i = \frac{\delta HA + \delta A^- \times 10^{(pHi - pKa)}}{1 + 10^{(pHi - pKa)}} \quad (1)$$

where δHA is the chemical shift of the carboxyl group of the fully protonated form and δA^- is that of the fully deprotonated form. The parameters δHA and δHA^- and the pKa value were obtained by the Gauss-Newton nonlinear least-squares fitting procedure on the basis of the experimental titration data. The pH values were the pH meter readings without correction for isotope effects [8].

Pulse sequences for the measurement of the $^1H-^{15}N$ NOE values, and the T_1 and T_2 relaxation times have been described elsewhere [9]. To improve the sensitivity and the water suppression, we applied the sensitivity enhancement with field gradient pulses in the Z-axis [10]. The ^{15}N T_1 values were determined from a series of $^1H-^{15}N$ correlation spectra with different relaxation durations, 32.94, 92.94, 172.94, 332.94, 652.94, 1292.94, and 1812.94 ms, while the T_2 values were determined from the spectra with durations of 4, 42, 82, 122, 202, 282, and 342 ms. We used a recycle delay of 4.0 s for the T_1 relaxation and 2.4 s for the T_2 relaxation experiments. The $^1H-^{15}N$ steady-state NOE values were determined from pairs of spectra, recorded with and without proton saturation. A recycle delay of 4.0 s was used for NOE experiments. All spectra were processed and analyzed using nmrPipe [11]. We used a series of extracted intensity profiles of each cross-peak for the extraction T_1 and T_2 relaxation time. We determined the steady-state $^1H-^{15}N$ NOE values from the ratios of the peak intensities with and without proton saturation. The relaxation data were analyzed using the model-free formalism by Lipari and Szabo [12, 13] and the extension of this method developed by Clore et al. [14, 15].

Enzymatic activity

We mixed 60 µl of PNP-$(GlcNAc)_5$ (0.06 mM) dissolved in the buffers 0.1 M sodium acetate (pH 2.0 – 5.0) or sodium phosphate (pH 5.5 – 8.0) with 30 µl of lysozyme solution (3 µM) dissolved in these buffers. The mixtures were then incubated at 37 °C. An aliquot (10 µl) was withdrawn at appropriate incubation intervals from the reaction mixture and analyzed by high-performance liquid chromatography, using a YMC-pack A-014 (6 × 300 mm) column developed with acetonitrile/water (80 : 20) eluent at a flow rate of 1 ml/min. The elution of PNP-$(GlcNAc)_5$ was detected by absorbance at 300 nm. The concentration of PNP-$(GlcNAc)_5$ was determined by calculating the area of an eluted peak [16].

Results and discussion

Characteristics of the solution structure

The resonance assignments of mouse lysozyme M were successfully performed by employing the 2D- and 3D-NMR spectra using the standard strategy. The $^1H-^{15}N$ NMR spectra of mouse lysozyme M were well dispersed. Most of the ^1H and ^{15}N polypeptide backbone resonances were assigned, but those of Lys1, Pro71, and Pro103 and some distal side chain ^1H resonances in arginines and lysines and side chain NH resonances of asparagines and glutamines were not assigned [5].

From 3D NOESY data, we obtained NOE connectivities. Figure 1 summarizes the NOE connectivities and H-D exchange experiments. Since NOE connectivities of d_{NN} (i, i+3), $d_{\alpha N}$(i, i+1), $d_{\beta N}$(i, i+3) , d_{NN}(i, i+2), $d_{\alpha N}$(i, i+4), and

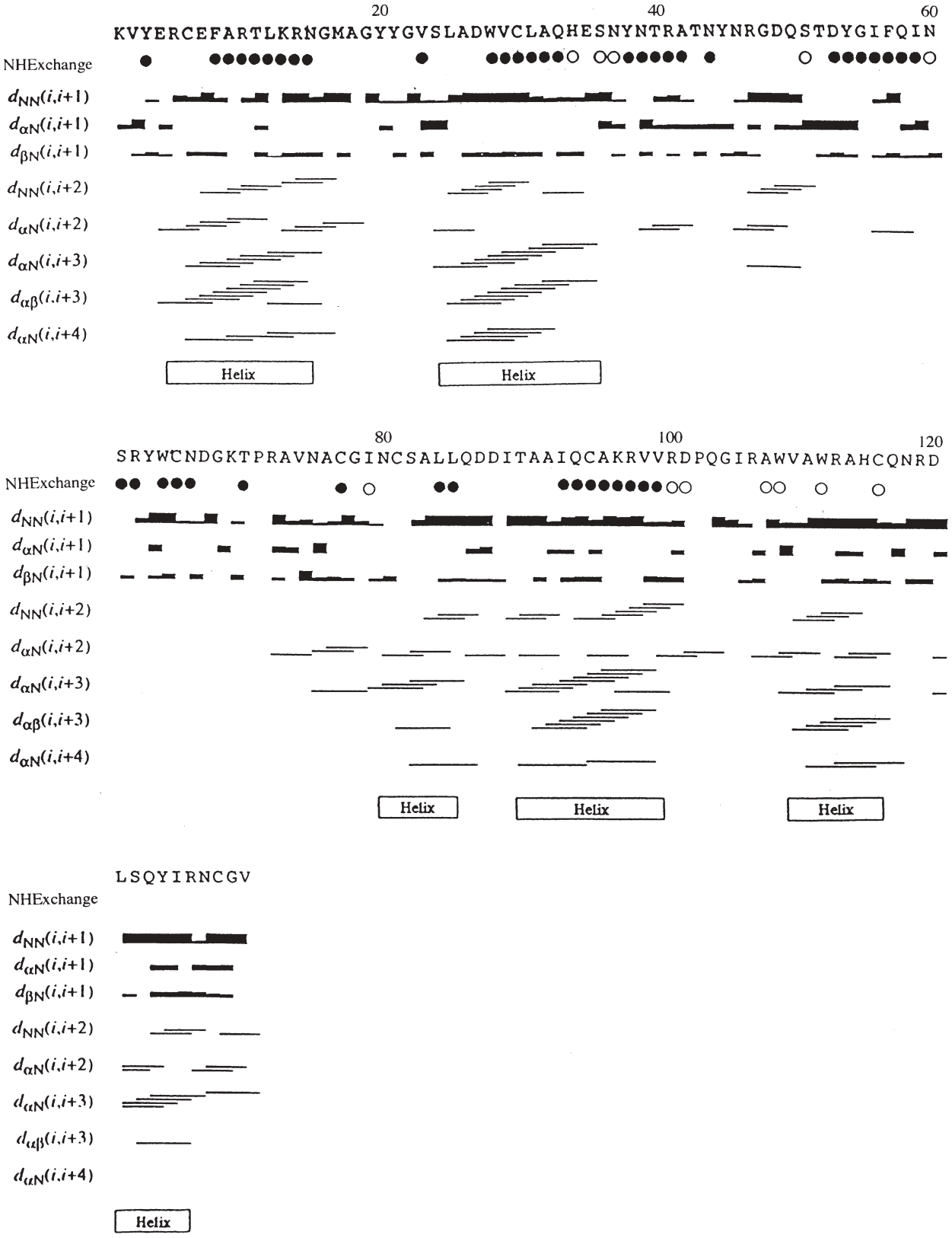

Figure 1. Short-range NOE connectivities for mouse lysozyme M. The NOE correlations were determined from 3D NOESY spectra recorded at 35 °C. The height of the bar indicates the strength of the NOE correlation. Slow and intermediate H-D exchange of backbone NH protons are indicated by filled circles and open circles, respectively.

$d_{\alpha\beta}$(i, i+3) indicate a feature of the α-helical structure [17], the positions of α-helices were assigned as Arg5–Arg14, Leu25–Ser36, Thr90–Val99, and Trp108–Arg115 (fig. 1). Next, since NOE connectivities of $d_{\alpha N}$ (i, i+2) and scarcity of NOE connectivities of $d_{\alpha N}$ (i, i+4) indicate a feature of a 3_{10} helical structure [17], the positions of 3_{10} helices were assigned as Asn80–Leu84 and Ser122–Ile125 (fig. 1). On the other hand, since NOE connectivities of $d_{\alpha N}$ (i, i+3), scarcity of NOE connectivities of d_{NN} (i, i+1), and medium- and long-range NOE indicate a feature of a β-sheet structure [17], the positions of β-sheet structures were assigned as Lys1–Tyr3 and Tyr38–Thr40 (double-stranded anti-parallel β-sheet) and Ala42–Asn46, Ser51–Gly55, and Ile59–Ser61 (triple-stranded anti-parallel β-sheet) (fig. 2). These secondary structures were consistent with those estimated from the backbone amide H-D exchange experiment (figs 1, 2).

We obtained NMR data for structure determination at pH 3.8, without added salt, at a temperature of 35 °C. Of the 300 NMR structures calculated, we selected a subset of the 20 lowest-energy structures for analysis (fig. 3; see also Materials and methods). The overall NMR structure consisted of four α-helices, two 3_{10} helices, and a double- and a triple-stranded anti-parallel β-sheet, consistent with the results in figures 1 and 2. The lowest root-mean-square deviation (RMSD) values are found in the regions containing regular secondary structures; the backbone RMSD between such regions was 0.77 ± 0.21 Å, while that calculated over all residues was 1.14 ± 0.27 Å. The N and C terminals and some loop regions were less defined, which may be due to both scarcity of NOE constraints and the conformational flexibility of the regions, which has been suggested in other globular proteins [19].

Next we compared the NMR structure of mouse lysozyme M with the X-ray structure [20] and NMR

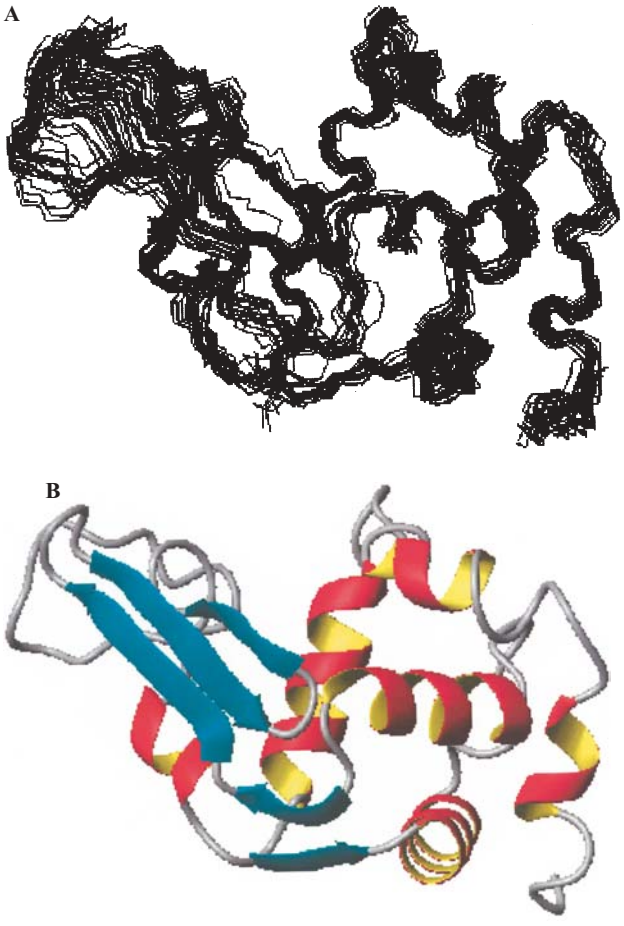

Figure 3. (*A*) Best-fit superposition of the backbone atoms of 20 structures of mouse lysozyme M: (*B*) Schematic ribbon representation of mouse lysozyme M. The diagrams were generated using the program MOLMOL [18].

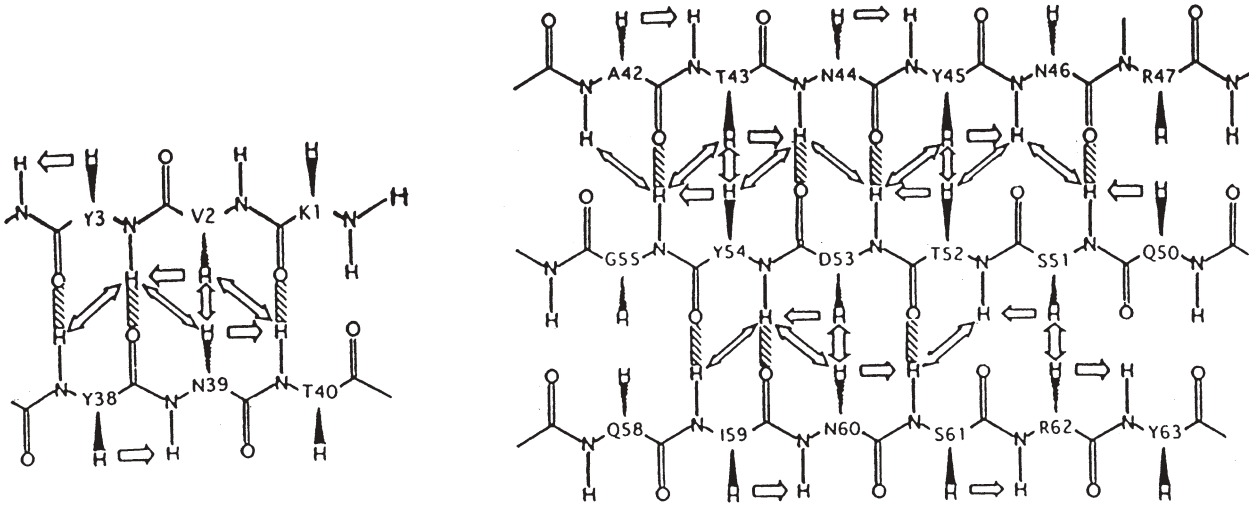

Figure 2. Representation of the backbone atoms of β-strands of mouse lysozyme M deduced from backbone NOE and amide protons with slow H-D exchange rates. Double-headed arrows denote sequential and interstrand connectivities. Hatched bars denote hydrogen bonding.

structure [21] of hen lysozyme. The average RMSD values calculated at the backbone atoms or at helix regions between the lowest-energy NMR structure of mouse lysozyme M and the X-ray structure or the NMR structure of hen lysozyme were 1.89 or 2.29 Å and 1.27 or 1.56 Å, respectively. Therefore, we concluded that the overall structure of mouse lysozyme M at pH 3.8 and 35 °C showed good agreement with that of hen lysozyme.

Enzymatic activity of mouse lysozyme M

Figure 4 shows the pH-activity profiles of PNP-$(GlcNAc)_5$ hydrolysis by mouse lysozyme M. For comparison, those by hen lysozyme whose enzymatic reaction mechanism has been investigated in detail are also shown in figure 4. The pH-activity profile of PNP-$(GlcNAc)_5$ hydrolysis by mouse lysozyme M was similar to that of hen lysozyme, but the hydrolytic activity of the former was lower. Figure 5 shows partial primary structures of hen and mouse lysozyme. The homology of the primary structure and tertiary structure of the backbone (described above) between hen and mouse lysozyme M indicates that the active residues in mouse lysozyme M are Glu35 and Asp53. To examine the pKa values of these residues in mouse lysozyme M, we measured 600 MHz DQF-COSY spectra at various pHs in the presence of 100 mM NaCl at 35 °C under the conditions in which pKa values of active residues in hen lysozyme were obtained. With a change of solution pH, the chemical shifts of cross-peaks from Glu35 and Asp52 in mouse lysozyme M on DQF-COSY spectra, which were assigned in our previous paper [5], changed. Using Eq. 1 in Materials and methods, we determined that the pKa values of Glu35 and Asp53 in mouse lysozyme M were 6.3 and 3.7, respectively, in the presence of 100 mM NaCl at 35 °C. Since the pKa values of Glu35 and Asp53 in hen lysozyme were 6.2 and 3.7, respectively, in the presence of 100 mM NaCl at 35°C, [7], we confirmed that the pH-activity profile of PNP-$(GlcNAc)_5$ hydrolysis by mouse lysozyme M was similar to that of hen lysozyme because the pKas of their active residues were nearly equal.

On the other hand, to analyze the reason for the lower activity of mouse lysozyme M, we measured the dissociation constant (K_d) of the mouse- and hen lysozyme-$(GlcNAc)_3$ complex at pH 5, at which their hydrolytic activities are optimum (table 1). The dissociation constant of the mouse lysozyme M-$(GlcNAc)_3$ complex was twice as great as that of the hen lysozyme-$(GlcNAc)_3$ complex.

Previously, we prepared Gln35 hen lysozyme, which had no activity [22]. That is, Gln35 hen lysozyme does not hydrolyze a hexamer of GlcNAc [$(GlcNAc)_6$], a lysozyme substrate, to a tetramer and dimer of GlcNAc. Therefore, we can determine the dissociation constant of the Gln35 hen lysozyme-$(GlcNAc)_6$ complex. Since the dissociation constant of the Gln35 hen lysozyme-$(GlcNAc)_6$ complex was nearly equal to that of the hen lysozyme-$(GlcNAc)_3$ complex [22], we estimated roughly the concentration of enzyme-substrate complex in the course of the hydrolytic reaction of PNP-$(GlcNAc)_5$ by lysozymes using the K_d of the lysozyme-$(GlcNAc)_3$ complex, PNP-$(GlcNAc)_5$ concentration, and lysozyme concentration at pH 5 and 37 °C. The percentages of enzyme-substrate complex concentration against enzyme concen-

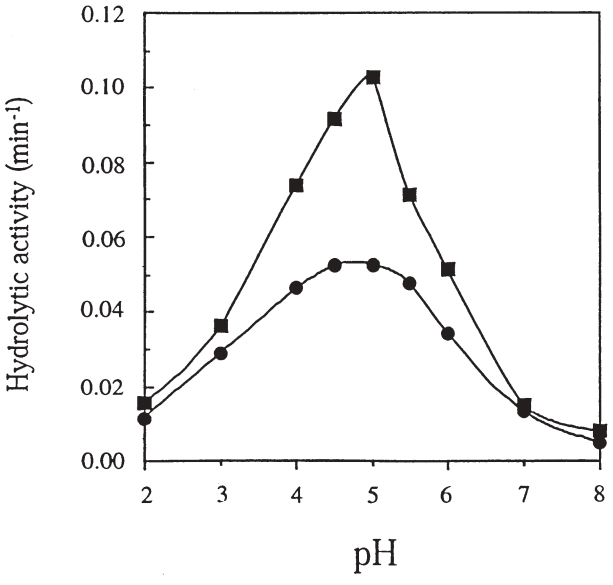

Figure 4. pH dependence of the hydrolytic reaction of PNP-$(GlcNAc)_5$ by mouse (filled circles) and hen (filled squares) lysozyme at 37 °C.

Table 1. Dissociation constant (K_d) of lysozyme-$(GlcNAc)_3$ complex at pH 5 and 37 °C.

Lysozyme	K_d (M)
Mouse	4×10^{-5}
Hen	2×10^{-5}

```
          30        40        50        60
Hen     -WVCAAKFESNFNTQATNRNT-DGSTDYGILQINSRWWCN-

Mouse   -WVCLAQHESNYNTRATNYNRGDQSTDTGIFQINSRYWCN-
          30        40        50        60
```

Figure 5. Partial primary structures of mouse and hen lysozyme.

tration were 66% for hen lysozyme and 50% for mouse lysozyme M. A rough estimation indicates that the hydrolytic activity of mouse lysozyme M was lower than that of hen lysozyme because of the larger dissociation constant of the mouse lysozyme M-substrate complex. However, since mouse lysozyme had half as much hydrolytic activity as hen lysozyme at pH 5, we tried to find another factor causing this difference in their hydrolytic activities. Recently, Mine et al. [4] in our laboratory suggested that the internal motions in hen lysozyme were related to its biological activity. Therefore, we also paid attention to the internal motions in mouse lysozyme M involved in biological functions such as substrate binding and enzyme catalysis.

Backbone dynamics of mouse lysozyme M

We obtained ^{15}N T_1, T_2, and heteronuclear NOE values of 117 out of 130 residues from NMR relaxation measurement of mouse lysozyme M in the absence of substrate analogue. Of the 13 uncharacterized residues, Lys1, Pro71, and Pro103 were not assigned [5]. The remaining 10 residues were excluded from the analysis due to severe spectral overlap. For most residues, the T_1, T_2, and NOE values appeared in the range 0.47–0.57 s, 120–150 ms, and 0.7–0.9, respectively. The T_1/T_2 ratios at residues throughout the protein were almost uniform, and we judged that the rotation of the molecule was isotropic. Moreover, the line-width of the ^{1}H-^{15}N HSQC spectrum of the protein was narrow. These results indicate that the protein exists as a monomer. The overall rotational correlation time (τ_c) was calculated using data of residues with T_1/T_2 ratios within 1 standard deviation from the mean value. The optimal τ_c for free mouse lysozyme M was calculated as 5.37 ns. We subsequently used these values (the T_1, T_2, and NOE values, and the τ_c value) to determine the internal dynamics parameters in terms of a so-called model-free approach [9, 10] and extensions thereof [14, 15]. Five models were considered, which included the following parameters: (1) S^2; (2) S^2 and τ_e; (3) S^2 and R_{ex}; (4) S^2, τ_e, and R_{ex}; (5) S_f^2, S_s^2, and τ_s. The model-free parameters for free mouse lysozyme M are shown in figure 6. These relaxation data for 117 residues could be fitted successfully to one of five optimal combinations of model-free parameters. For most residues, the order parameters (S^2) were in the range 0.80–0.95; a mean S^2 value of 0.87 ± 0.03 was calculated over all residues, indicating that rapid motions on the fast (pico- to nanosecond) time scale were largely restricted. However, the order parameters (S^2) were much lower for strand 1 (residues 42–47) and the following turn (residues 42–50), the long loop (residues 65–75), the loop before the helix (residues 85–89), and the loop after the helix (residues 117–120), indicating that these regions are flexible. These S^2 profiles were consistent with the RMSD profiles of backbone atoms of the 20 native structures (fig. 3).

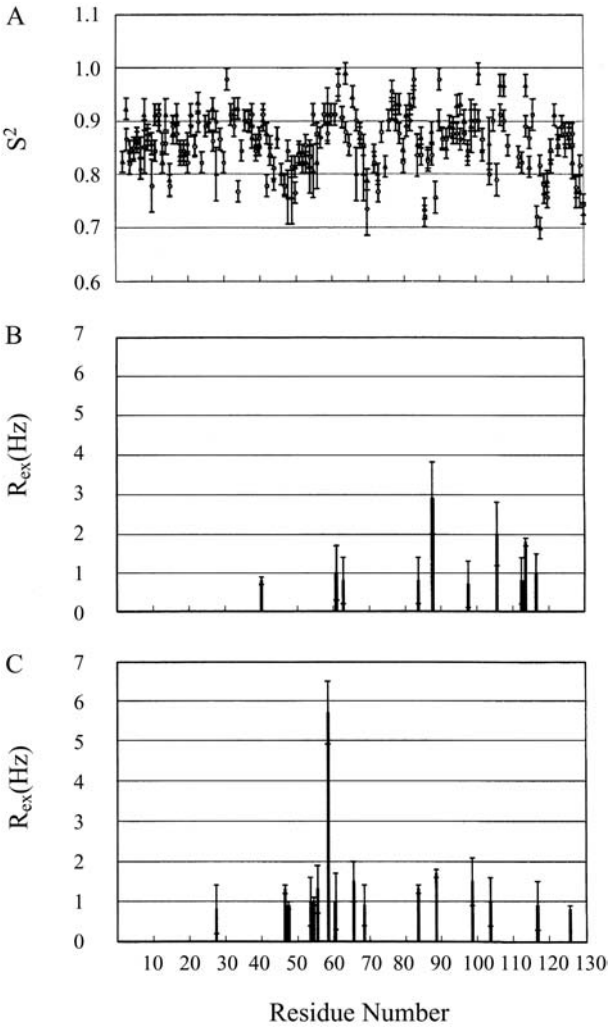

Figure 6. Extracted model-free parameters of mouse lysozyme M by parameter optimization with the program RxAnly. (*A*) Comparison of the generalized order parameters (S^2) for free mouse lysozyme M (open circles) and for ligand-bound mouse lysozyme M (closed triangles): (*B*) Chemical exchange contributions represented in the broadened line-width (R_{ex}) for free mouse lysozyme M: (*C*) Chemical exchange contributions represented in the broadened line-width (R_{ex}) for ligand-bound mouse lysozyme M.

The backbone dynamics of hen lysozyme have been reported [4, 23]. The order parameters of mouse lysozyme M are similar to those of hen lysozyme. The primary sequence similarity of mouse lysozyme M to hen lysozyme was 56.9%, but the overall structure of mouse lysozyme M was almost identical to hen lysozyme, as described above. Therefore, the global conformation rather than the amino acid sequence seems to dominate the internal motions of the protein.

In the presence of $(GlcNAc)_3$ where most of the mouse lysozyme M molecules form an enzyme-substrate complex, ^{15}N T_1, T_2, and heteronuclear NOE values of 102 out of 130 residues were obtained. Of the 28 uncharacterized residues, Lys 1, Pro71, and Pro103 were not assigned [5].

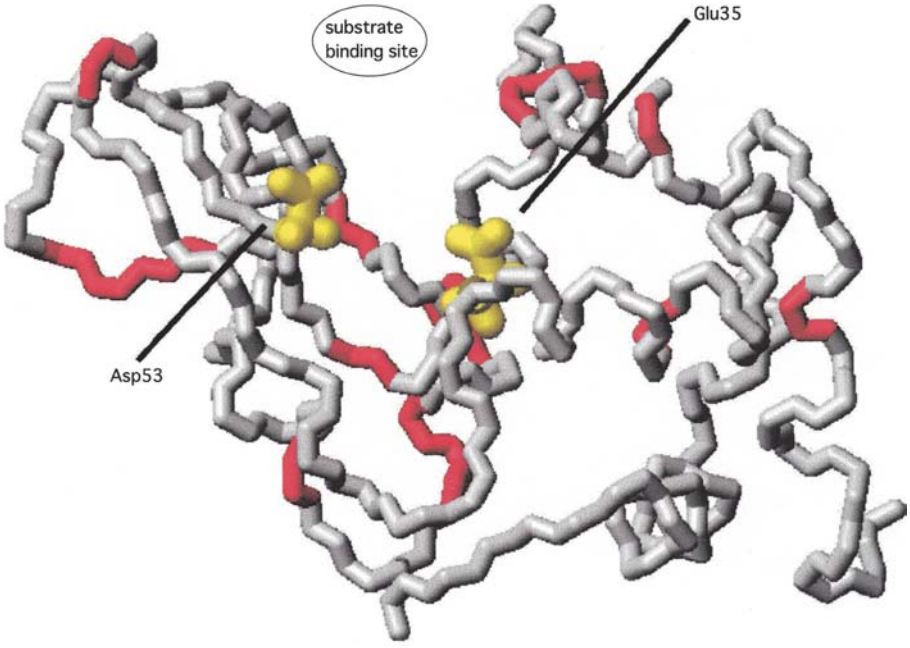

Figure 7. Tertiary structure representation of mouse lysozyme M with the significant changes in chemical shift (more than 0.05 ppm) (red) on the formation of complex with substrate analogue. Active-site residues, Glu35 and Asp52, are shown in yellow.

The remaining 25 residues were excluded from the analysis due to severe spectral overlap and extreme line broadening due to the presence of substantial chemical exchange. Such line-broadening effects in hen lysozyme might arise from either the existence of multiple binding sites or from exchanges in the motion of these residues on binding [24]. We plotted residues whose resonances shifted more than 0.05 ppm in the presence of $(GlcNAc)_3$ in the overall structure of mouse lysozyme M (fig. 7). The residues were located in the cleft where active-site residues, Glu35 and Asp53, faced each other. Small changes in chemical shift were observed in regions remote from the active site, indicating that the effects of inhibitor binding are felt throughout the enzyme. Such an observation occurred in hen lysozyme with the addition of $(GlcNAc)_3$, which was interpreted as due to a small conformational change in the cleft on the formation of lysozyme-substrate complex [24].

The optimal τ_c for ligand-bound mouse lysozyme M was calculated as 5.51 ns, and the model-free analysis was carried out using these relaxation parameters as described above (fig. 6). For most residues, the order parameters were in the range 0.80–0.95, indicating that rapid motions in ligand-bound protein were restricted, as with the free protein. However, there were some residues that changed the internal motions upon binding of $(GlcNAc)_3$. Increases in order parameters were located at the Asn66 and Asp67 residues in the long loop, at the Arg101, Arg107, and Ala108 residues in the loop, and at the Ala114 residue in the loop after the helix. On the other hand, decreases in order parameters were located at the Trp28 residue in the helix, at the Gly68 residue in the long loop, and at the Asn118 residue in the loop after the helix. The present data showing that order parameters decreased or increased upon ligand binding were consistent with the internal motions of ligand-bound hen lysozyme [4] .

On the other hand, R_{ex} values were observed at some residues around the active-site cleft, especially Ile59, upon binding. R_{ex} values reflect the existence of a dynamic exchange from a microsecond to millisecond time scale.

These motions were considered to be related to the biological function of lysozyme, because the number of residues showing R_{ex} values in the mutant hen lysozyme, which has a hydrolytic activity higher than the wild-type hen lysozyme, increased significantly [4]. This means that the more the lysozyme molecule shows fluctuation from a microsecond to millisecond time scale, the higher the lysozyme enzymatic activity. We therefore compared the number of residues showing R_{ex} values in the mouse lysozyme M-$(GlcNAc)_3$ complex with that of the hen lysozyme-$(GlcNAc)_3$ complex. In the hen lysozyme-$(GlcNAc)_3$ complex, R_{ex} values were observed at residues Phe3, Trp28, Glu35, Gln41, Ala42, Arg45, Asn46, Asp52, Tyr53, Gly54, Cys64, Asn65, Arg68, Cys76, Asn77, Cys80, Ser81, Ile88, Lys96, Cys115, and Leu129 [4]. The number of residues showing R_{ex} values in the mouse lysozyme M-$(GlcNAc)_3$ complex was clearly less than that in the hen lysozyme-$(GlcNAc)_3$ complex, indi-

cating that the mouse lysozyme M molecule on the formation of the $(GlcNAc)_3$ complex showed less fluctuation than hen lysozyme. Based on these results, we suggest that the lower hydrolytic activity of mouse lysozyme M compared to hen lysozyme may be due to the restriction of internal motions from the microsecond to millisecond time scale.

Comparison of mouse lysozyme M with human lysozyme

The primary sequence similarity of mouse lysozyme M to human lysozyme was 77.7%, since these lysozymes are both from mammals, so we also compared mouse lysozyme M with human lysozyme. The average RMSD values calculated at the backbone atoms or at helix regions between the NMR structure of the lowest-energy mouse lysozyme M and the X-ray structure of human lysozyme [25] were 1.73 and 1.12 Å, respectively. The finding that the average RMSD values between mouse lysozyme M and human lysozyme were lower than those between mouse lysozyme M and hen lysozyme showed that the primary sequence similarity was closely involved in the global conformation.

Human lysozyme had a higher activity than hen lysozyme against glycol chitin, a soluble polymer of GlcNAc [26], so we compared the number of residues showing R_{ex} values in the mouse lysozyme M-$(GlcNAc)_3$ complex with that of the human lysozyme-$(GlcNAc)_3$ complex, reported elsewhere [27]. In the human lysozyme-$(GlcNAc)_3$ complex, R_{ex} values were observed at residues Trp34, Thr43, Tyr45, Asn46, Ala47, Gly48, Asp49, Gly55, Ile56, Ser61, Arg62, Ala76, Cys77, Ala83, Leu84, Ile89, Val93, Gln104, Ile106, Ala108, Asn114, Cys115, and Asn118 [27]. The number of residues showing R_{ex} values in the mouse lysozyme M-$(GlcNAc)_3$ complex (fig. 6) was less than in the human lysozyme-$(GlcNAc)_3$ complex, indicating that the mouse lysozyme M molecule showed less fluctuation than human lysozyme upon the formation of the $(GlcNAc)_3$ complex. The result was consistent with the result obtained by comparing hen lysozyme and mouse lysozyme M.

Conclusion

We investigated the solution structure and backbone dynamics of mouse lysozyme M using heteronuclear NMR methods. The NMR structures indicated that the global fold of mouse lysozyme M was quite similar to those of hen lysozyme in solution and in the crystalline state. The hydrolytic activity of mouse lysozyme M against PNP-$(GlcNAc)_5$ was lower than that of hen lysozyme. We suggest that the reason for the lower activity of mouse lysozyme M was the larger dissociation constant of the mouse lysozyme M-substrate complex than that of the hen lysozyme-substrate complex and the more restricted internal motion from a microsecond to millisecond time scale in mouse lysozyme M.

Acknowledgements. The authors thank Dr. Shin-ichi Tate (Department of Structural Biology, Biomolecular Engineering Research Institute) for providing pulse sequence and data analysis programs and Dr. D. Khoda (Medical Institute of Bioregulation, Kyushu University) for valuable discussion in determining the solution structure of mouse lysozyme M. We also thank KN-international (USA) for improvement of our English. This work was supported in part by a grant from the Sapporo Bioscience Foundation.

1 Imoto T., Johnson L. N., North A. T. C., Phillips D. C. and Rupley J. A. (1972) Vertebrate lysozyme, In: The Enzyme, vol. 7, pp. 665–868, Boyer P. D. (ed.), New York, Academic Press
2 Cross M., Mangelsdorf I., Wedel A. and Renkawitz R. (1988) Mouse lysozyme M gene: isolation, characterization, and expression studies. Proc. Natl. Acad. Sci. USA **85:** 6232–6236
3 Tsujihata Y., So T., Chijiiwa Y., Hashimoto Y., Hirata M., Ueda T. et al. (2000) Mutant mouse lysozyme carrying a minimal T cell epitope of hen egg lysozyme evokes high autoantibody response. J. Immunol. **165:** 3606–3611
4 Mine S., Tate S., Ueda T., Kainosho M. and Imoto T. (1999) Analysis of the relationship between enzyme activity and its internal motion using nuclear magnetic resonance: ^{15}N relaxation studies of wild-type and mutant lysozyme. J. Mol. Biol. **286:** 1547–1565
5 Obita T., Ueda T., Tanaka Y., Hashimoto Y. and Imoto T. (2000) Assignment of ^{1}H and ^{15}N resonances of mouse lysozyme M. J. Biomol. NMR **18:** 361–362
6 Guntert P., Mumenthaler C. and Wüthrich K. (1997) Torsion angle dynamics for NMR structure calculation with the new program DYANA. J. Mol. Biol. **273:** 283–298
7 Bartik K., Redfield C. and Dobson C. M. (1994) Measurement of the individual pKa values of acidic residues of hen and turkey lysozymes by two dimensional ^{1}H NMR. Biophys. J. **66:** 1180–1184
8 Bundi A. and Wüthrich, K. (1983) ^{1}H NMR parameters of the common amino-acid residues measured in aqueous solutions of the linear tetrapeptides H-Gly-Gly-X-Ala-OH. Biopolymers **18:** 285–297
9 Kay L. E., Torchia D. A. and Bax A. (1989) Backbone dynamics of proteins as studied by ^{15}N inverse detected heteronuclear NMR spectroscopy: application to staphylococcal nuclease. Biochemistry **28:** 8972–8979
10 Kay L. E., Keifer P. and Saarinen T. (1992) Pure absorption gradient enhanced heteronuclear single quantum correlation spectroscopy with improved sensitivity. J. Am. Chem. Soc. **114:** 10663–10665
11 Delaglio F., Grzesiek S., Vuister G.W., Zhu G., Pfeifer J. and Bax A. (1995) NMRPipe: a multidimensional spectral processing system based on UNIX pipes. J. Biomol. NMR **6:** 277–293
12 Lipari G. and Szabo A. (1982) A model-free approach to the interpretation of nuclear magnetic resonance relaxation macromolecules. I. Theory and range of validity. J. Am. Chem. Soc. **104:** 4546–4559
13 Lipari G. and Szabo A. (1982) A model-free approach to the interpretation of nuclear magnetic resonance relaxation macromolecules. II. Theory and range of validity. J. Am. Chem. Soc. **104:** 4559–4570
14 Clore G. M., Szabo A., Bax A., Kay L. E., Driscoll, P. C. and Gronenborn A. M. (1990) Deviations from the simple two-parameter model-free approach to the interpretation of nitrogen-15 nuclear magnetic relaxation of protein. J. Am. Chem. Soc. **112:** 4989–4991

15 Clore G. M., Driscoll P. C., Wingfield P. T. and Gronenborn A. M. (1990) Analysis of the backbone dynamics of interleukin-1 beta using two-dimensional inverse detected heteronuclear ^{15}N-^{1}H NMR spectroscopy. Biochemistry **29:** 7387–7401
16 Kumagai I., Maenaka K., Sunada F., Takeda S. and Miura K. (1993) Effects of subsite alterations on substrate-binding mode in the active site of hen egg-white lysozyme. Eur. J. Biochem. **212:** 151–156
17 Wüthrich K. (1986) NMR of Proteins and Nucleic Acids, New York, Wiley
18 Koradi R., Billeter M. and Wüthrich K. (1996) MOLMOL: a program for display and analysis of macromolecular structures. J. Mol. Graph. **14:** 51–55
19 Powers R., Clore G. M., Garrett D. S. and Gronenborn A. M. (1993) Relationships between the precision of high-resolution protein NMR structures, solution-order parameters, and crystallographic B factors. J. Magn. Reson. B. **101:** 325–327
20 Vaney M. C., Maignan S., RiesKautt M. and Ducruix A. (1996) High-resolution structure (1.33-Å) of a hew lysozyme tetragonal crystal growth in the APCF apparatus – data and structural comparison with a crystal growth under microgravity from Spacehab-01 mission. Acta. Crystallogr. D. Biol. Crystallogr. **52:** 505–517
21 Schwalbe H., Grimshaw S. B., Spencer A., Buck M., Boyd J., Dobson C. M. et al. (2001) A refined solution structure of hen lysozyme determined using residual dipolar coupling data. Protein Sci. **10:** 677–688
22 Kuroki R., Yamada H., Moriyama T. and Imoto T. (1986) Chemical mutations of the catalytic carboxyl groups in lysozyme to the corresponding amides. J. Biol. Chem. **261:** 13571–13574
23 Buck M., Boyd J., Redfield C., MacKenzie D. A., Jeenes D. J., Archer D. B. et al. (1995) Structural determinants of protein dynamics: analysis of ^{15}N NMR relaxation measurements for main-chain and side-chain nuclei of hen egg white lysozyme. Biochemistry **34:** 4041–4055
24 Lumb K. J., Cheetham J. C. and Dobson C. M. (1994) ^{1}H nuclear magnetic resonance studies of hen lysozyme-N-acetylglucosamine oligosaccharide complexes in solution: application of chemical shifts for the comparison of conformational changes in solution and in the crystal. J. Mol. Biol. **235:** 1072–1087
25 Artymiuk P. J. and Blake C. C. F. (1981) Refinement of human lysozyme at 1.5 Å resolution analysis of non-bonded and hydrogen-bond interactions. J. Mol. Biol. **152:** 737–762
26 Kuramitsu S., Ikeda K., Hamaguchi K., Fujio H. and Amano T. (1974) Ionization constants of Glu 35 and Asp 52 in hen, turkey, and human lysozymes. J. Biochem. **76:** 671–683
27 Mine S., Ueda T., Hashimoto Y. and Imoto T. (2000) Analysis of the internal motion of free and ligand-bound human lysozyme by use of ^{15}N NMR relaxation measurement: a comparison with those of hen lysozyme. Protein Sci. **9:** 1669–1684